Received: 1 October 2016 | Revised: 12 May 2017 | Accepted: 14 June 2017

DOI: 10.1002/rnc.3885

RESEARCH ARTICLE

WILEY

Dynamic modeling and nonlinear tracking control of a novel modified quadrotor

Mohamad Ali Tofigh | Mohamad J. Mahjoob | Moosa Ayati

School of Mechanical Engineering, College of Engineering, University of Tehran, Tehran, Iran

Correspondence
Mohamad J. Mahjoob, School of Mechanical Engineering, College of Engineering, University of Tehran, PO Box 11155-4563, Tehran, Iran.
Email: mmahjoob@ut.ac.ir

Summary

In this article, a nonlinear tracking controller is designed based on Lyapunov stability for a novel aerial robot. The proposed 6-rotor configuration improves stability and payload lifting capacity of the robot compared with conventional quadrotors while avoiding further complexities in the robot dynamics and steering principles. The dynamical model of the robot is derived using Newton-Euler method. The model represents a nonlinear, coupled, and underactuated system. The proposed control strategy includes 2 main parts: an attitude controller and a position controller. Both the attitude and position controls are Lyapunov-based nonlinear tracking controllers that guarantee the asymptotic convergence of the states' tracking errors to zero. Simulation results are presented to illustrate appropriate performance of the closed-loop system in terms of position/attitude tracking even in the presence of wind disturbance.

KEYWORDS

lyapunov controller, modified quadrotor, nonlinear control, novel aerial robot

1 | INTRODUCTION

Several autonomous robots have been developed including ground (wheeled, tracked, or legged) and aerial vehicles. Ground robots, however, have inherent limitations due to the terrain complexities and presence of obstacles. Aerial robots are therefore preferred to perform many tasks/missions in exploration, defense, and even daily applications.[1] Quadrotors, in particular, carry out a wide range of civil applications such as terrain and utilities inspection, disaster monitoring, environmental surveillance, search and rescue, wild fire surveillance, aerial mapping and cinematography, agricultural spraying, and traffic controlling.

In a general classification, aerial robots are divided into 4 categories of fixed-wing, rotary-wing, ships, and flapping robots. Among these, rotary and fixed-wing robots have more operational applications than others. Rotary-wing robots with vertical take-off/landing ability and hover flight capabilities form a large and important class of aerial robots. Additionally, these robots have a better maneuverability over other types, which enhance the feasibility of their application. In this very class, the "quadrotor" is an ideal platform for robotic systems particularly suited for the development and testing of new control strategies because of simple mechanical structure, easy steering principle, and ability to hover.[2]

A quadrotor is an aerial robot that utilizes 4 fixed-pitch rotors to propel the vehicle. This type of configuration will facilitate the control, as the movement of the robot is controlled by changing the speed of the propellers.

Various flight control systems have been presented for quadrotors. Linear methods have been successfully applied to quadrotors in Bouabdallah et al[3] and Salih et al[4]; however, these methods can only guarantee stability of the closed-loop system for small regions around the equilibrium point and are restricted to large/fast maneuvers, where the linearity of the

system is not a valid assumption. Many nonlinear controllers have also been proposed for trajectory tracking. One may quote the feedback linearization,[5,6] Back-stepping approach,[7,8] sliding mode method,[9,10] robust and adaptive techniques,[11,12] and some intelligent controllers.[13,14]

Quadrotors face 2 challenges of stability and payload capacity. A rotary-wing robot will become more stable and efficient once the rotor area is increased.[15] Therefore, the designed aerial robots tend to have more rotors in order to improve the stability of the vehicle. However, such rotors impose some complexity and lead to the limitation of the robot's maneuverability.

A number of modified configurations have been suggested to improve the performance of quadrotors. A hexa-copter[16] and an octa-copter[17] with all rotors distributed symmetrically on both sides of the fuselage were proposed. A 4-rotor configuration that merges the simplicity of a quadrotor with the energy efficiency of a helicopter was also presented.[18] This class of aerial robots, called "triangular quadrotor," consists of a single fixed-pitch main rotor with 3 smaller rotors on booms that provide both counter-torque and maneuvering control. In Cao and Anvar,[19] a 5-rotor configuration is designed, which uses rotor speed control for orientation control. The main deficiency of the proposed configurations is that dynamics and steering of the vehicles have become more complicated than conventional quadrotors.

In this article, a novel configuration is presented aimed at increasing stability and payload lifting capacity of the quadrotor. The configuration is designed in a way that the dynamics and steering principles are kept as simple as conventional quadrotors. The modified quadrotor has 2 additional coaxial rotors in the center, rotating in a constant speed and opposite directions (Figure 1). The motion control is carried out by the 4 peripheral rotors, like a conventional quadrotor. In other words, speed of these motors varies during flight, whereas the coaxial rotors spin in constant values.

The additional coaxial propellers increase rotor area and improve the stability accordingly. Two coaxial propellers are completely identical and rotate at constant speeds in opposite directions. As a result, the gyroscopic and drag torques of each propeller will be eliminated. These rotors do not therefore impose any extra term in the dynamics of the vehicle. On the other hand, the thrust produced by each of the coaxial propellers is in the same direction, helping the robot to carry heavier payloads. Also, in this modified configuration, a major portion of the payload weight is compensated by coaxial rotors causing the 4 controlling motors rotate at lower speeds. Compare it with a conventional quadrotor in which all the payload weight is carried by the 4 motors forcing the rotors to rotate at much higher speeds.

Attempts are made here first to model the dynamics and then control this new vehicle. The mathematical model that describes the motion of the modified quadrotor is derived by the Newton-Euler formulation. The equations are fully nonlinear, coupled, unstable, and underactuated. Control synthesis based on Lyapunov approach is a well-known technique for nonlinear systems because it guarantees the stability of the closed-loop system. In this work, a nonlinear trajectory tracking control system based on Lyapunov function with hierarchical structure is presented.

This article is projected as follows. Section 2 lays out the mathematical model describing the modified quadrotor dynamics. Section 3 describes how the physical parameters of the real robot are measured experimentally. In Section 4, the control objectives and controller design procedure are explained. Simulation results illustrating the performance of the proposed control strategy are presented in Section 5, and Section 6 concludes the article.

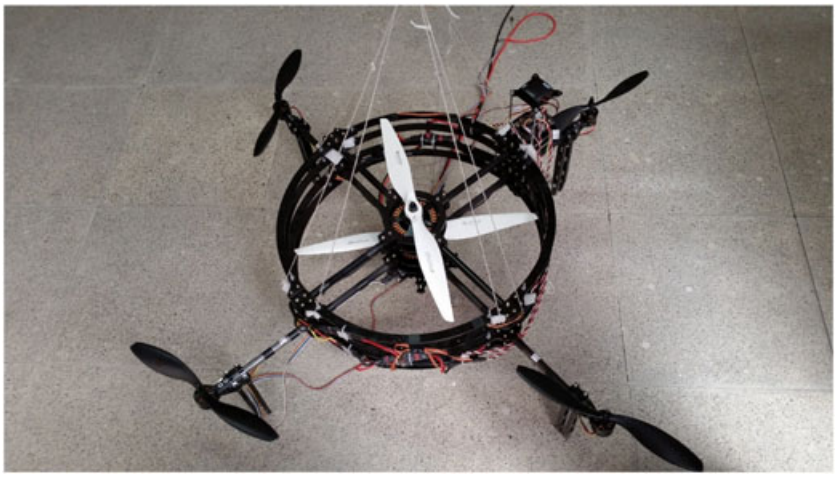

FIGURE 1 Modified quadrotor portrait [Colour figure can be viewed at wileyonlinelibrary.com]

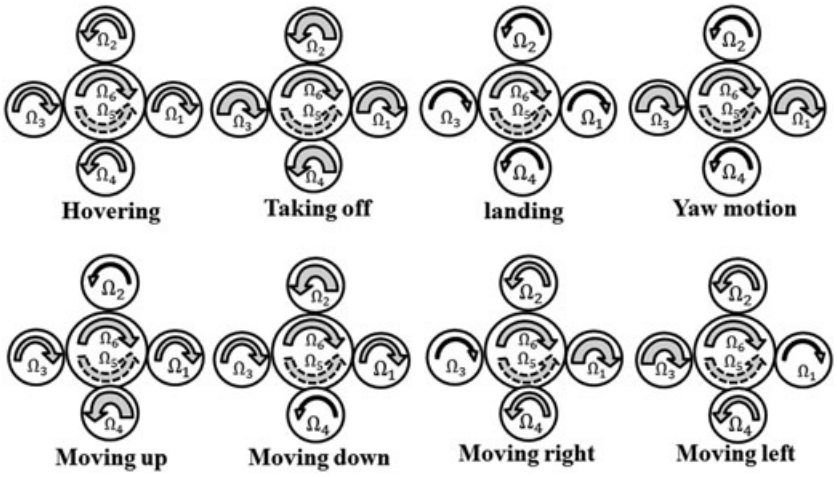

FIGURE 2 The modified quadrotor operating principles: The relationship between propeller speeds and vehicle moments

2 | DYNAMICAL MODEL

2.1 | Modified quadrotor system description

The very rules governing the maneuvers of the modified quadrotor are illustrated in Figure 2. The basic maneuvers are achieved by varying the speed of 4 controlling motors, which change the force and torque balances acting on the vehicle. As mentioned before, the coaxial rotors have equal and constant speeds during all maneuvers. The dynamic model of this modified configuration can be derived as follows.

2.2 | Kinematics

Figure 3 shows the kinetics/kinematics of the modified quadrotor. The dynamical model is set upon the body-frame B (O_{xyz}) and the earth-frame E (O_{XYZ}). Let vector $\boldsymbol{P} = [X, Y, Z]^{'}$ denotes the position of the center of gravity of the quadrotor in the earth-frame, whereas vector $\boldsymbol{\omega} = [p, q, r]^{'}$ represents its angular velocity in the body-frame. The orientation of the robot is given by the rotation matrix R: $E \rightarrow B$, where R depends on the 3 Euler angles, that is, roll (φ), pitch (θ)), and yaw (ψ). These angles are bounded by $(-\frac{\pi}{2} < \varphi, \theta < \pi/2)$ and $(-\pi < \psi < \pi)$. The rotation matrix is then obtained as follows:

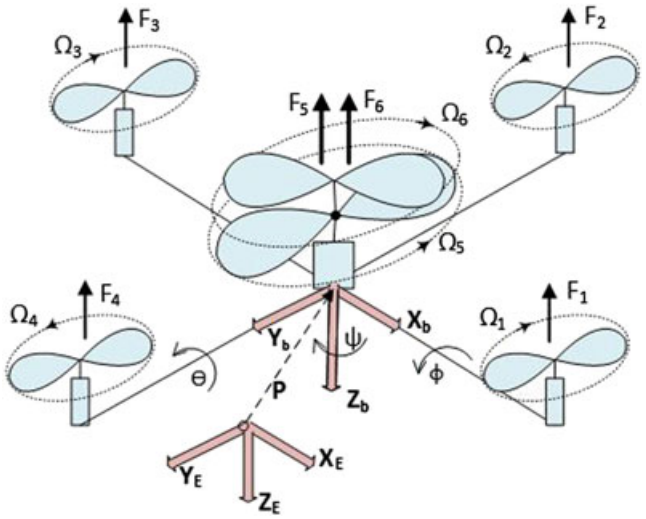

FIGURE 3 Kinematics and kinetics configuration of the modified quadrotor [Colour figure can be viewed at wileyonlinelibrary.com]

$$
\begin{aligned}
R(x,\varphi) &= \begin{bmatrix} 1 & 0 & 0 \\ 0 & cos\ \varphi & \sin\varphi \\ 0 & -\sin\varphi & \cos\varphi \end{bmatrix} \\
R(y,\theta) &= \begin{bmatrix} \cos\theta & 0 & -\sin\theta \\ 0 & 1 & 0 \\ \sin\theta & 0 & \cos\theta \end{bmatrix} \\
R(z,\psi) &= \begin{bmatrix} \cos\psi & \sin\psi & 0 \\ -\sin\psi & \cos\psi & 0 \\ 0 & 0 & 1 \end{bmatrix} \\
R(\psi,\theta,\varphi) &= R(x,\varphi).R(y,\theta).R(z,\psi)
\end{aligned} \tag{1}
$$

The kinematic equations of rotational and translation motions are obtained through the rotation matrix. The translational kinematics is stated as $\boldsymbol{v_B = R\,.\,v_E}$, where $v_E = [u_E, v_E, w_E]'$ and $v_B = [u_b, v_b, w_b]'$ are linear velocities of the mass center expressed in the earth-frame and body-frame, respectively. Consequently, the rotational kinematics is obtained from the relationship between the rotation matrix and its derivative as follows:

$$
\begin{aligned}
\begin{bmatrix} p \\ q \\ r \end{bmatrix} &= \begin{bmatrix} 0 \\ 0 \\ \dot{\psi} \end{bmatrix} + R(z,\psi)\begin{bmatrix} 0 \\ \dot{\theta} \\ 0 \end{bmatrix} + R(z,\psi)\times R(y,\theta)\begin{bmatrix} \dot{\varphi} \\ 0 \\ 0 \end{bmatrix} \\
\begin{bmatrix} p \\ q \\ r \end{bmatrix} &= \begin{bmatrix} \cos\theta\cos\psi & \sin\psi & 0 \\ -\cos\theta\sin\psi & \cos\psi & 0 \\ \sin\theta & 0 & 1 \end{bmatrix}\begin{bmatrix} \dot{\varphi} \\ 0 \\ \dot{\psi} \end{bmatrix}
\end{aligned} \tag{2}
$$

2.3 | Kinetics

The thrust generated by each propeller is given by

$$F_i = K_t \Omega_i^2 \tag{3}$$

The reaction torque caused by the drag generated by each propeller is

$$T_i = -K_d \Omega_i^2 \tag{4}$$

where Ω_i's correspond to the propellers angular velocities ($i = 1,..,6$), and $K_t > 0$ and $K_d > 0$ are the thrust and reaction torque coefficients, which depend on the air density, the radius of the propeller, the number of blades, and the geometry.[20] These parameters are measured experimentally (see Section 3).

The total force/torque vector produced by the propellers is given by

$$
\begin{bmatrix} F \\ \tau_\varphi \\ \tau_\theta \\ \tau_\psi \end{bmatrix} = \begin{bmatrix} K_t & K_t & K_t & K_t & K_t' & K_t' \\ LK_t & 0 & -LK_t & 0 & 0 & 0 \\ 0 & -LK_t & 0 & LK_t & 0 & 0 \\ -K_d & K_d & -K_d & K_d & K_d' & -K_d' \end{bmatrix}\begin{bmatrix} \Omega_1^2 \\ \Omega_2^2 \\ \Omega_3^2 \\ \Omega_4^2 \\ \Omega_5^2 \\ \Omega_6^2 \end{bmatrix} \tag{5}
$$

where L denotes the distance from the center of each controlling propeller to the robot center of mass. The translational movement is expressed in the earth-frame by the following equation:

$$m_t\ddot{\boldsymbol{P}} = \boldsymbol{f} \tag{6}$$

where m_t represents the total mass of the robot, and the vector $\boldsymbol{f}$ represents the resultant of external forces applied to the robot due to gravity and aerodynamic effects of both the propellers and the vehicle. Substituting the state vector $\mathbf{P}$ into Equation 6 yields:

$$\begin{cases} \ddot{X} = \dfrac{1}{m_t}\left(F\sin\theta - k_1\dot{X}\right) \\ \ddot{Y} = \dfrac{1}{m_t}\left(-F\sin\varphi\cos\theta - k_2\dot{Y}\right) \\ \ddot{Z} = \dfrac{1}{m_t}\left(-F\cos\varphi\cos\theta + m_t\, g - k_3\dot{Z}\right) \end{cases} \tag{7}$$

The last terms in the above equation are aerodynamic forces in which $[k_1, k_2, k_3]$ are the drag coefficients. Considering that the vehicle is a rigid body and also symmetric, the rotational kinetic equation in the body-frame is expressed as follows:

$$\mathbf{M} = \boldsymbol{I}\dot{\boldsymbol{\omega}} + \boldsymbol{\omega}\times\boldsymbol{I}\boldsymbol{\omega} \tag{8}$$

where $\boldsymbol{I} = diag[I_x\, I_y\, I_z]$ denotes the inertia matrix of the robot, and $\mathbf{M}$ represents the total torque provided by propellers and aerodynamic effects.

The additional gyroscopic torque caused by the motor, rotor, and the propeller is given by

$$\boldsymbol{\tau_g} = \sum\boldsymbol{\omega}\times\boldsymbol{H_i} \tag{9}$$

where $\boldsymbol{H_i}$ is the angular momentum. It only appears in the z axis because of the angular velocity once the motor rotates. The angular momentum then follows the relation $\boldsymbol{H_i} = [0\ 0\ J_r\Omega_i]'$, where J_r refers to the inertia of the propeller about the z axis. According to the above relations, the total torque is obtained as follows.

$$\boldsymbol{M} = \boldsymbol{\tau_g} + \begin{bmatrix} \tau_\varphi \\ \tau_\theta \\ \tau_\psi \end{bmatrix} + \boldsymbol{\tau_{drag}} \tag{10}$$

Invoking Equations 8 to 10, the rotational governing equations of the robot are

$$\begin{cases} \dot{p} = \dfrac{1}{I_x}\left(\left(I_y - I_z\right)qr - J_r q\Omega + \tau_x - k_4\, p\right) \\ \dot{q} = \dfrac{1}{I_y}\left(\left(I_z - I_x\right)pr + J_r p\Omega + \tau_y - k_5\, q\right) \\ \dot{r} = \dfrac{1}{I_z}\left(\left(I_x - I_y\right)pq + \tau_z - k_6 r\right) \end{cases} \tag{11}$$

where $\{k_4, k_5, k_6\}$ are the drag coefficients with positive constant, and $\Omega = \Omega_1 - \Omega_2 + \Omega_3 - \Omega_4$ is the overall residual propeller angular velocity. Notice that since during the flight $\Omega_5 = -\Omega_6$, the sum of gyroscopic and drag torque components of the coaxial propeller is zero (ie, the coaxial propellers do not have no effect on the dynamics of the robot).

Equations 7 and 11 describe translational and rotational motions of the 6-rotor aerial robot (modified quadrotor) in the earth-frame and body-frame, respectively. These equations (which are similar to the dynamic equations of a quadrotor) are still complicated for control synthesis. Therefore, some simplification is carried out to make the control easier. Let $[p,\ q,\ r]' = \left[\dot{\varphi},\ \dot{\theta},\ \dot{\psi}\right]'$ according to Lara et al[21] and Wang and Jia[22]; thus, the dynamic equation can be written in a simple form as follows:

$$\begin{cases} \ddot{X} = \frac{1}{m_t}\left(u_1 \sin\theta - k_1\dot{X}\right) \\ \ddot{Y} = -\frac{1}{m_t}\left(u_1 \sin\varphi\cos\theta + k_2\dot{Y}\right) \\ \ddot{Z} = \frac{1}{m_t}\left(-u_1\cos\varphi\cos\theta + m_t g - k_3\dot{Z}\right) \\ \ddot{\Phi} = \frac{1}{I_x}\left(\left(I_y - I_z\right)\dot{\psi}\dot{\theta} - J_r\dot{\theta}\Omega - k_4\,\dot{\varphi} + u_2\right) \\ \ddot{\theta} = \frac{1}{I_y}\left(\left(I_z - I_x\right)\dot{\psi}\dot{\varphi} + J_r\dot{\varphi}\Omega - k_5\,\dot{\theta} + u_3\right) \\ \ddot{\psi} = \frac{1}{I_z}\left(\left(I_x - I_y\right)\dot{\varphi}\dot{\theta} - k_6\dot{\psi} + u_4\right). \end{cases} \tag{12}$$

where the control inputs are defined as $[u_1,\ u_2,\ u_3,\ u_4]' = [F,\ \tau_x,\ \tau_y,\ \tau_z]'$. The robot has 6 DOF as $[\varphi, \theta, \psi, X, Y, Z]'$ and 4 inputs, so the system is underactuated; only 4 outputs can be controlled directly. In this work, position (**P**) and heading angle (ψ) of the aerial robot are chosen as outputs.

The actual input signals that should be computed are the speeds of motors. Given the control inputs obtained from the control system, the speed of each motor is calculated as

$$\begin{cases} \Omega_1^2 = \frac{u_1 - K_t'\left(\Omega_5^2 + \Omega_6^2\right)}{4k_t} - \frac{u_3}{2lk_t} - \frac{u_4}{4k_d} \\ \Omega_2^2 = \frac{u_1 - K_t'\left(\Omega_5^2 + \Omega_6^2\right)}{4k_t} - \frac{u_2}{2lk_t} + \frac{u_4}{4k_d} \\ \Omega_3^2 = \frac{u_1 - K_t'\left(\Omega_5^2 + \Omega_6^2\right)}{4k_t} + \frac{u_3}{2lk_t} - \frac{u_4}{4k_d} \\ \Omega_4^2 = \frac{u_1 - K_t'\left(\Omega_5^2 + \Omega_6^2\right)}{4k_t} + \frac{u_2}{2lk_t} + \frac{u_4}{4k_d} \end{cases} \tag{13}$$

where the speeds of both coaxial propellers are the same, computed according to the weight of payload. They are constant during the flight as well.

3 | EXPERIMENTAL MEASUREMENT OF SYSTEM PARAMETERS

In others to design the control system and get valid simulation results, it was necessary to obtain accurate values of the physical parameters used in the dynamic model. In this section, we report the experimental measurements conducted to determine the main parameters of the system such as mass, moments of inertia, and aerodynamic coefficient of the propeller.

3.1 | Mass and moments of inertia

The total mass of the robot, without any payload, was 2.45 kg (measured by a calibrated scale). Moment of inertia can be computed analytically by summing the contributions of all individual components of the robot; however, this is often complicated to apply into the robot assembly.[23] Here, the 2-wire torsional test is used to determine the robot moment of inertia.[24]

The method consists of the test object (robot) suspended by 2 thin wires that have the same lengths (Figure 4). The robot oscillates about the vertical axis by giving a small initial angle, and the period of oscillation is recorded. The simplified equation of oscillating movement is obtained by assuming that the angular motion is small and neglecting the damping as follows:

$$\ddot{\psi} + \frac{cdW}{I_z H}\psi = 0 \tag{14}$$

where c and d are displacements from center of gravity, H indices the height, and W refers to the weight. The period of oscillations is as follows:

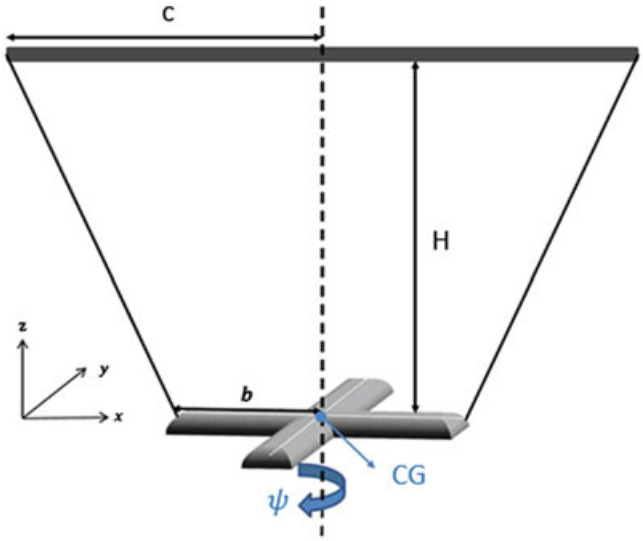

FIGURE 4 Schematic of the 2-wire torsional test [Colour figure can be viewed at wileyonlinelibrary.com]

$$T = 2\pi\sqrt{\frac{I_z H}{cdW}} \tag{15}$$

The moment of inertia can therefore be calculated from Equation 15.

For accurate results, the experiments were carried out at different heights (H). The data were measured for 10 oscillations and 4 tests for each H. The results are shown in Table 1. Taking the last row in Table 1 as the time period (T), the moment of inertia is calculated from Equation 15; the average gives us $I_z = 0.056$ kgm^2. The moments of inertia about other axes (listed in Table 2) were obtained similarly.

3.2 | Aerodynamics effects of propeller

As mentioned, movement of the flying robot is managed by changing the speeds of the 4 controlling motors. Referring to Equation 13, computing these speeds depends on the control inputs (u_1~ u_4) discussed in the following section and also thrust and reaction torque coefficient of each propeller.

The relationship between thrust and the reaction torque with speed of each rotor is described in Equations 3 and 4. The test setup, shown in Figure 5, was designed to measure the aerodynamic factors of each propeller experimentally. The setup consisting of a load cell, an optical tachometer, and a microcontroller measures both the thrust and the reaction torque factors. The electric propulsion system of the robot is composed of BLDC motor, electronic speed controller, and propeller. The 2 coaxial BLDC motors are T-motor U8 with 18″ propeller, and the 4 controlling motors are x-Aircraft, attached to 12″ propellers. The speed of the BLDC motors is recorded by a tachometer.

Using the configuration shown in Figure 5A, the load cell measures the force proportional to the thrust of propeller. In the other configuration (Figure 5B), the output of the load cell is proportional to the reaction torque of the propeller.

TABLE 1 Results of Measuring Moment of Inertia About z Axes

Height	$H = 0.45$ m	$H = 0.65$ m
Test1	2.432 s	2.966 s
Test2	2.436 s	2.954 s
Test2	2.454 s	2.961 s
Test2	2.441 s	2.958 s
Average/10	0.244 s	0.296 s
I_z	0.0784 kgm^2	0.0798 kgm^2

TABLE 2 Robot Moments of Inertia About x, y, and z Axes

	Value	Unit
I_x	0.038	kgm^2
I_y	0.033	kgm^2
I_z	0.079	kgm^2

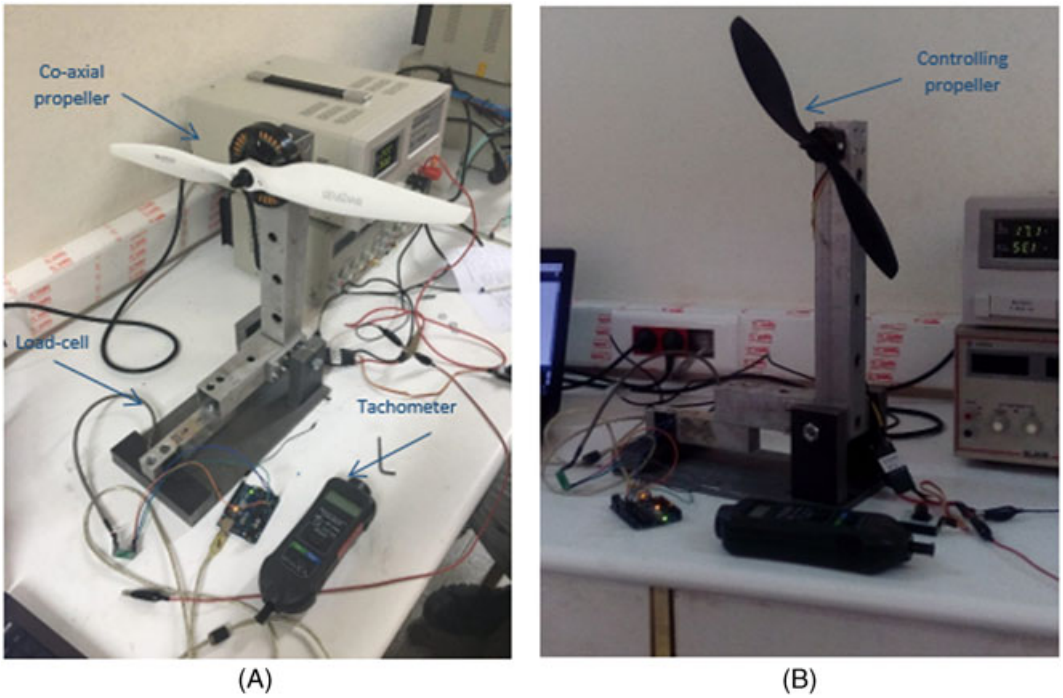

FIGURE 5 Setup for measuring aerodynamic coefficient of propellers: A, thrust B, reaction torque [Colour figure can be viewed at wileyonlinelibrary.com]

In order to find the thrust and reaction torque factors, the load-cell output is recorded at different speeds of the rotor measured by optical tachometer. Figure 6 displays the typical test results on one of the controlling rotors. For more accurate result, the data are obtained from 10 tests (for each speed), and the mean value is used in the plots. The test results are collected in Table 3.

4 | CONTROL SYNTHESIS

The modified quadrotor is an underactuated system; however; one can see from Equation 12 that the rotational dynamics is independent from translation dynamics, whereas the translation dynamics depends on roll (θ) and pitch (φ) angles. Therefore, the hierarchical control strategy is an appropriate alternative to control the system.[25] The block diagram of such a structure is schematically shown in Figure 7. According to the hierarchical control strategy, position and attitude dynamics are controlled in 2 separated loops. The position controller produces the desired attitude signals θ_d and φ_d f for θ and φ to track based on tracking errors of the longitudinal and latitudinal positions X and Y, respectively. It also creates input u1 to track the elevation reference Z_d for the Z position. The attitude controller will be applied to track the reference signals θ_d, φ_d, and ψ_df for the 3 attitude angles. In brief, altitude and attitude subsystems are controlled by using the inputs $u_1 \sim u_4$, and XY position is controlled by varying the θ and φ angles.

In this section, because of extreme nonlinearity in dynamics of the robot, a nonlinear tracking controller (based on Lyapunov stability theorem) is developed for both position and attitude subsystems.

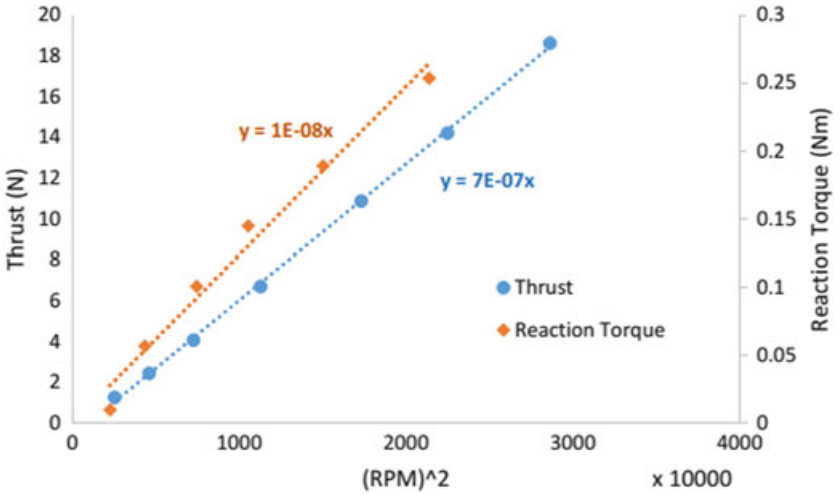

FIGURE 6 Thrust and reaction torque factors of controlling rotors [Colour figure can be viewed at wileyonlinelibrary.com]

TABLE 3 Aerodynamic Coefficients of Propellers

	Controlling Propeller	Coaxial Propeller
Thrust factor	k_t = 7e–7	$k_t^{'} = 8e{-}6$
Reaction torque factor	k_d = 1e–8	$k_d^{'} = 4e{-}7$

4.1 | Position controller design

Invoke Equations 12, and introduce virtual inputs as $u_x = \sin\theta$ and $u_y = \sin\varphi\cos\theta$, the translation dynamics will be full-actuated; the tracking errors are then defined as follows:

$$\begin{cases} e_1 = X - X_d \\ e_2 = \dot{X} - \dot{X}_d + \alpha_1(X - X_d) \\ e_3 = Y - Y_d \\ e_4 = \dot{Y} - \dot{Y}_d + \alpha_2(Y - Y_d) \\ e_5 = Z - Z_d \\ e_6 = \dot{Z} - \dot{Z}_d + \alpha_3(Z - Z_d) \end{cases} \tag{16}$$

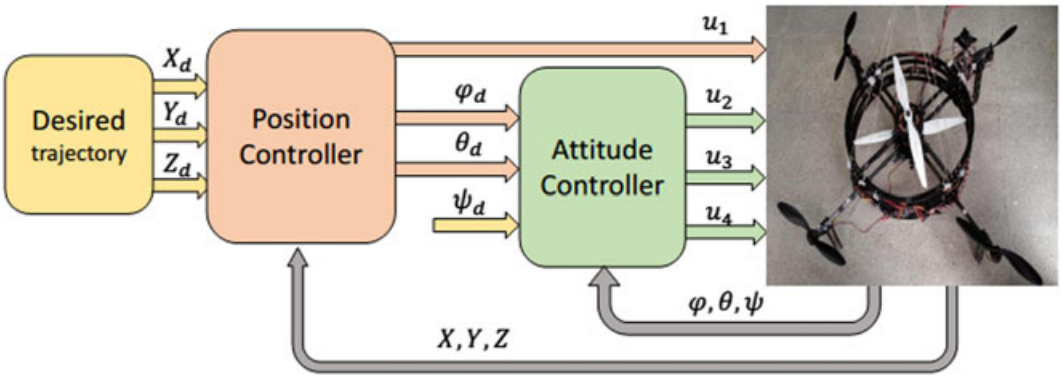

FIGURE 7 Control system architecture of the modified quadrotor [Colour figure can be viewed at wileyonlinelibrary.com]

A candidate positive definite Lyapunov function (V_1) is defined to check the stability of position controller as follows:

$$\boldsymbol{V}_1 = \frac{1}{2}\left(\boldsymbol{e}_1^2 + \boldsymbol{e}_2^2 + \boldsymbol{e}_3^2 + \boldsymbol{e}_4^2 + \boldsymbol{e}_5^2 + \boldsymbol{e}_6^2\right) \tag{17}$$

The time derivative of the $V_1$is is as

$$\dot{\boldsymbol{V}}_1 = \boldsymbol{e}_1\dot{\boldsymbol{e}}_1 + \boldsymbol{e}_2\dot{\boldsymbol{e}}_2 + \boldsymbol{e}_3\dot{\boldsymbol{e}}_3 + \boldsymbol{e}_4\dot{\boldsymbol{e}}_4 + \boldsymbol{e}_5\dot{\boldsymbol{e}}_5 + \boldsymbol{e}_6\dot{\boldsymbol{e}}_6 \tag{18}$$

Referring to Equations 12 and 18, the position controller is now designed as

$$u_x = \frac{m_t}{u_1}\left(\ddot{X}_d - \left(1-\alpha_1^2\right)e_1 - (\alpha_2+\alpha_1)e_2 + \frac{k_1}{m_t}\dot{X}\right) \tag{19}$$

$$u_y = \frac{m_t}{u_1}\left(\ddot{Y}_d - \left(1-{\alpha_3}^2\right)e_3 - (\alpha_4+\alpha_3)e_4 + \frac{k_2}{m_t}\dot{Y}\right) \tag{20}$$

$$u_1 = \frac{-m_t}{\cos\varphi\cos\theta}\left(-g + \ddot{Z}_d - \left(1-{\alpha_5}^2\right)e_5 - (\alpha_6+\alpha_5)e_6 + \frac{k_3}{m_t}\dot{Z}\right) \tag{21}$$

where $\{\alpha_1, \ldots, \alpha_6\}$ are controller parameters to be selected positive. Therefore, the time derivative of the Lyapunov function V_1i in Equation 18 becomes definitely negative except in the origin as

$$\dot{V}_1 = -\alpha_1{e_1}^2 - \alpha_2{e_2}^2 - \alpha_3{e_3}^2 - \alpha_4{e_4}^2 - \alpha_5{e_5}^2 - \alpha_6{e_6}^2 \leq 0 \tag{22}$$

According to Lyapunov stability theorem, asymptotic stability of the position errors is now guaranteed, and X, Y, and Z positions converge to the desired values: X_d, Y_d, Z_d in finite time.

The desired angles, which are sent to attitude control loop as the references signals, will be computed as follows:

$$\theta_d = \sin^{-1}\left(\frac{m_t}{u_1}\left(\ddot{X}_d + z_1 - \alpha_1^2 z_1 - \alpha_2 z_2 + \frac{k_1}{m_t}\dot{X}\right)\right) \tag{23}$$

$$\varphi_d = \sin^{-1}\left(-\frac{m_t}{u_1\cos\theta_d}\left(\ddot{Y}_d + z_3 - \alpha_3^2 z_3 - \alpha_4 z_4 + \frac{k_2}{m_t}\dot{Y}\right)\right) \tag{24}$$

4.2 | Attitude controller design

The attitude control of the quadrotor is the crucial part for stabilization and tracking control. A Lyapunov-based controller is designed for the 3 attitude angles to follow the reference signals θ_d, φ_d, , and ψ_d. Errors associated with the attitude dynamics of the modified quadrotor are defined as

$$\begin{cases} e_7 = \varphi - \varphi_d \\ e_8 = \dot{\varphi} - \dot{\varphi}_d + \lambda_1(\varphi - \varphi_d) \\ e_9 = \theta - \theta_d \\ e_{10} = \dot{\theta} - \dot{\theta}_d + \lambda_2(\theta - \theta_d) \\ e_{11} = \psi - \psi_d \\ e_{12} = \dot{\psi} - \dot{\psi}_d + \lambda_3(\psi - \psi_d) \end{cases} \tag{25}$$

The candidate Lyapunov function

$$V_2 = \frac{1}{2}\left(e_7^2 + e_8^2 + e_9^2 + e_{10}^2 + e_{11}^2 + e_{12}^2\right) \tag{26}$$

is now proposed. The attitude controller is then formulated to generate

$$u_2 = \left(I_z - I_y\right)\dot{\psi}\dot{\theta} + J_r\dot{\theta}\Omega + k_4\,\dot{\varphi} + I_x\left(\ddot{\varphi}_d - \left(1-\lambda_1{}^2\right)e_6 - \left(\lambda_2+\lambda_1\right)e_7\right)\right) \tag{27}$$

$$u_3 = \left(I_x - I_z\right)\dot{\psi}\dot{\varphi} - J_r\dot{\varphi}\Omega + k_5\,\dot{\theta} + I_y\left(\ddot{\theta}_d - \left(1-\lambda_3{}^2\right)e_8 - \left(\lambda_4+\lambda_3\right)e_9\right)\right) \tag{28}$$

$$u_4 = \left(I_y - I_x\right)\dot{\varphi}\dot{\theta} - k_6\dot{\psi} + I_z\left(\ddot{\psi}_d - \left(1-\lambda_5{}^2\right)e_{10} - \left(\lambda_5+\lambda_3\right)e_{11}\right) \tag{29}$$

The time derivative of the Lyapunov function (Equation 26) becomes negative definite by choosing positive values for controller parameters $\{\lambda_1,..,\lambda_6\}$, ; therefore

$$\dot{V}_2 = -\lambda_1 e_7{}^2 - \lambda_2 e_8{}^2 - \lambda_3 e_9{}^2 - \lambda_4 e_{10}{}^2 - \lambda_5 e_{11}{}^2 - \lambda_6 e_{12}{}^2 \leq 0 \tag{30}$$

Therefore, under the designed control strategy specified by Equations 27 to 29, the asymptotic convergence of the attitude angels to the desired values of $\varphi_d, \theta_d, \psi_d$ is guaranteed according to Lyapunov theory.

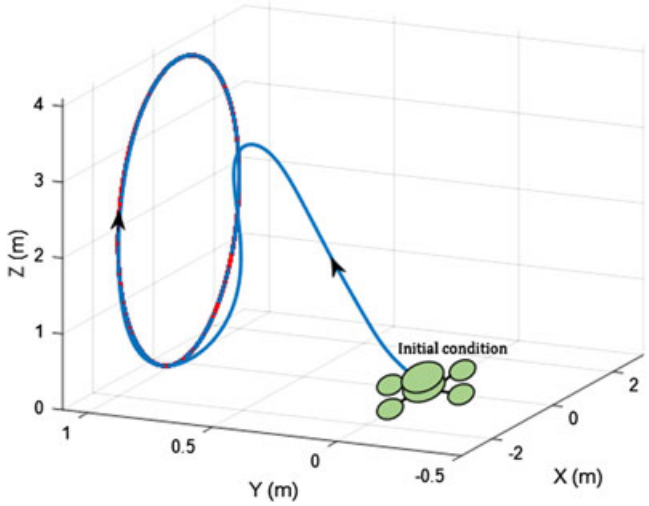

FIGURE 8 Path following in 3D-Cartesian space [Colour figure can be viewed at wileyonlinelibrary.com]

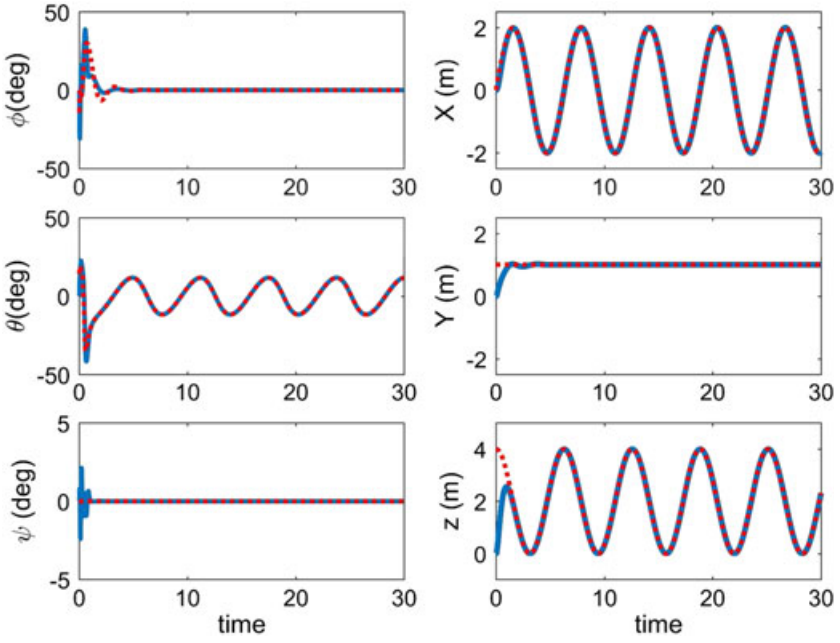

FIGURE 9 The positions (X, Y, Z) and Euler angles (φ, θ, ψ) [Colour figure can be viewed at wileyonlinelibrary.com]

5 | SIMULATION RESULTS

In order to prove the effectiveness of the proposed method, 2 simulation studies have been conducted to verify tracking features and robustness against disturbance. The simulations are carried out in MATLAB/SIMULINK, on an Intel-based PC equipped with Core i7-2670QM CPU with 8 GB of RAM and 500-GB SSD.

Main points considered during simulations follow:

(i) The simulation takes into account the full nonlinear model of the modified quadrotor presented in Equation 12.
(ii) The control inputs u_1 to u_4 are obtained by applying the controller proposed in Section 4.
(iii) The speed of each rotor is calculated using Equation 13.

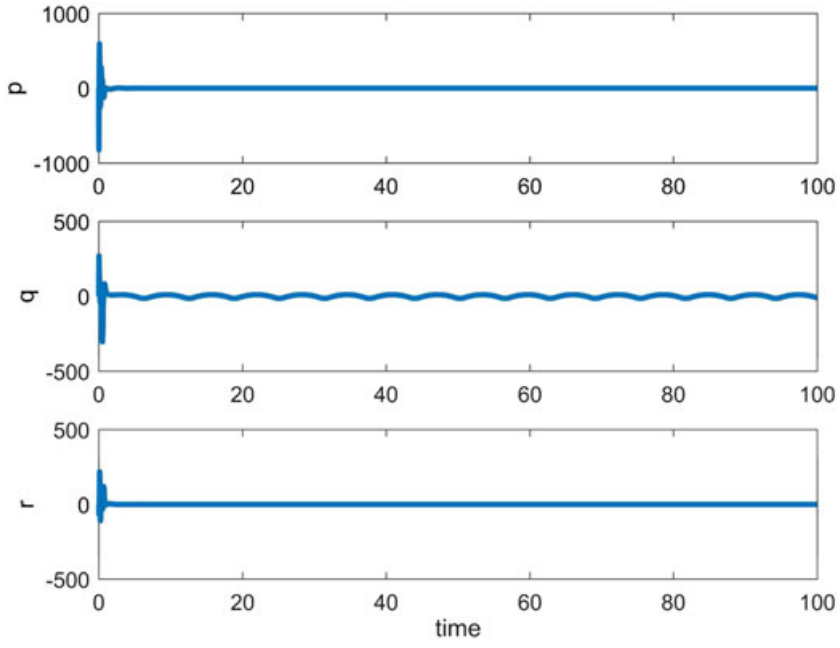

FIGURE 10 The angular velocities (p, q, r) [Colour figure can be viewed at wileyonlinelibrary.com]

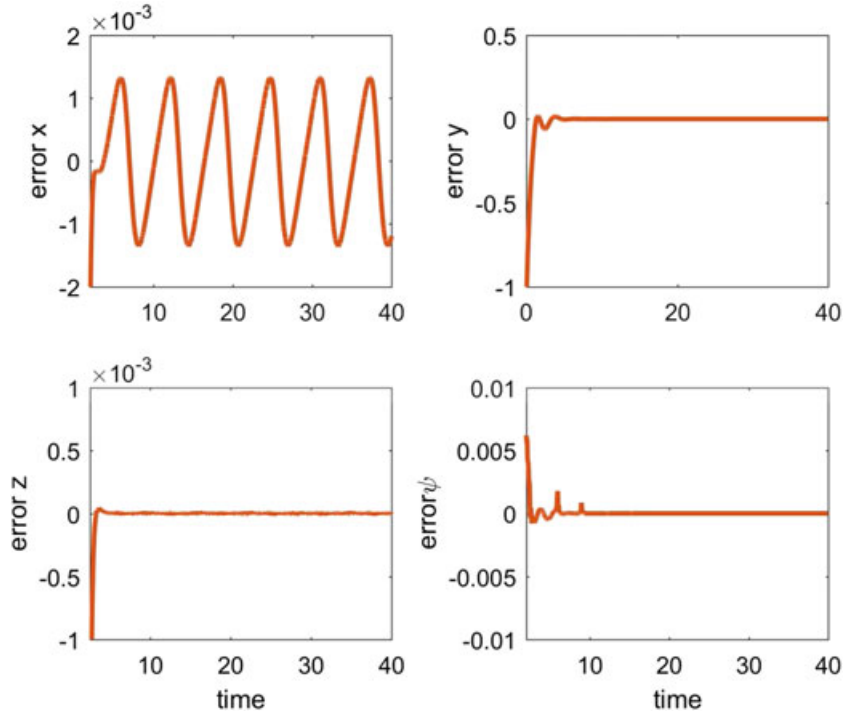

FIGURE 11 The tracking errors [Colour figure can be viewed at wileyonlinelibrary.com]

(iv) The controller parameters are chosen as $\alpha_1=\alpha_3=\alpha_5=2.8\,,\alpha_2=\alpha_4=\alpha_6=3.75\,,\lambda_1=\lambda_3=\lambda_5=15.94\,,\lambda_2=\lambda_4=\lambda_6=52.42.$

(v) We assumed that the coaxial propellers carry 2 kg of the weight (1 kg for the main vehicle plus 1-kg payload); therefore, $\Omega_5^2=\Omega_6^2=3479\ rpm$

Furthermore, the parameters of modified quadrotor determined experimentally in Section 3 represent typical real flying condition in a controlled environment.

5.1 | Simulation study subject to desired position tracking

The control task here is to stabilize the attitude of robot while tracking a desired position. The initial position and angle values of the modified quadrotor for the simulation tests are [0, 0, 0] m and [0, 0, 0] rad. The mission in this simulation is carrying a 1-kg payload and moving it on a circular path in the *ZX* plane defined by:

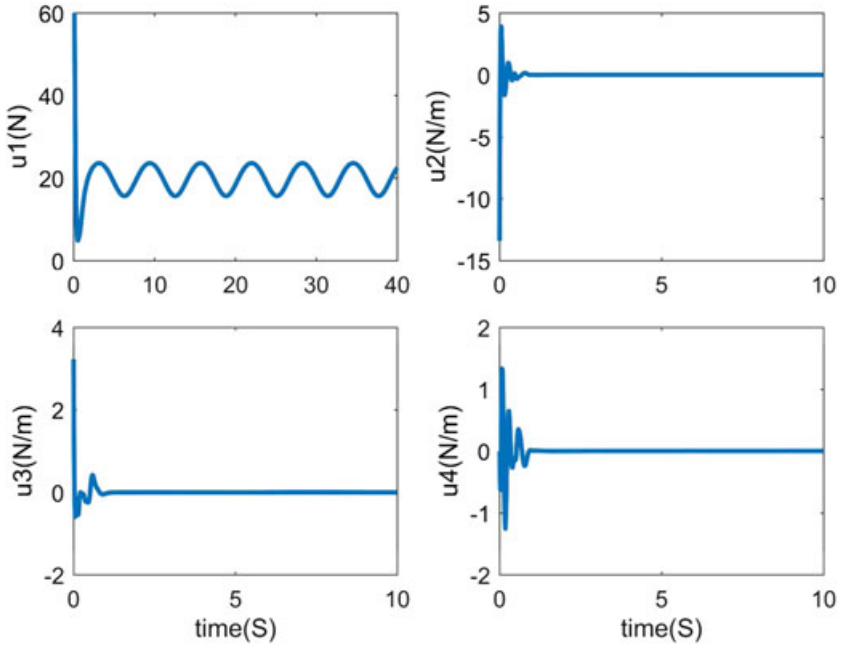

FIGURE 12 The controller inputs [Colour figure can be viewed at wileyonlinelibrary.com]

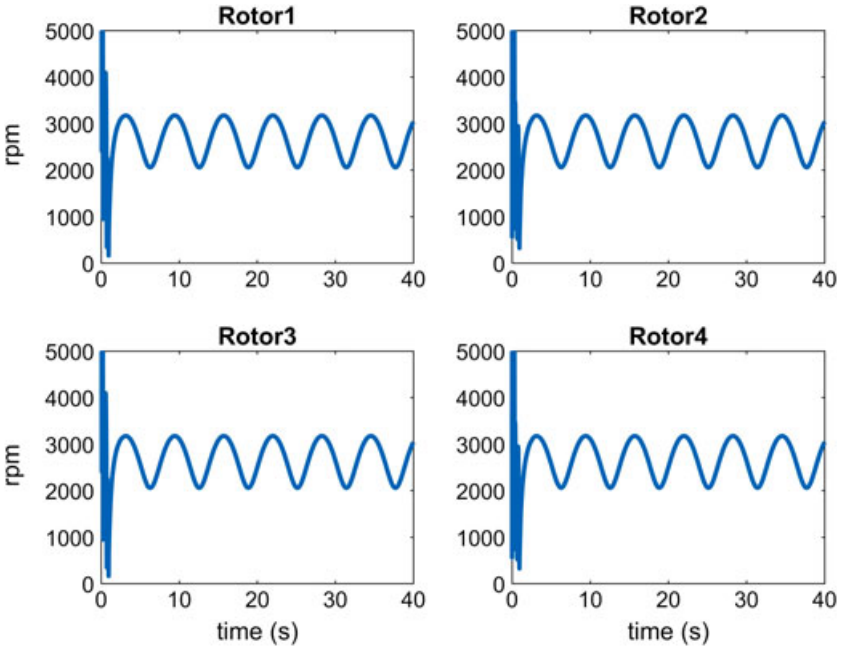

FIGURE 13 The speed of controlling rotors [Colour figure can be viewed at wileyonlinelibrary.com]

$$X_d = 2\sin(t), Y_d = 1, Z_d = 2 + 2\cos(t)$$

The desired heading angle (ψ_d) is set to zero. Figure 8 shows how the system approaches the desired path and stay on it; starting from an initial position far from the reference. As it is observed from Figures 9 and 10, the control scheme forces all the state variables to accurately follow the command signal with suitable transient characteristics. As the position controller generates smooth curves of the references θ_d and φ_d, the attitude controller could appropriately follow the desired signals (Figure 9). This portrays the main advantage of the hierarchical control strategy applied to the underactuated system. Figure 11 shows that all the output tracking errors approach zero.

The input signals produced by the proposed controllers are illustrated in Figure 12. The speed of each motor during the flight is shown in Figure 13. One can readily observe that the obtained speeds are continuous, smooth, and admissible for typical brushless motors/actuators. Because the coaxial rotors compensate a major part of the robot weight, the mean speeds of the controlling rotors remain at low values. This eventually provides a safer flight for the vehicle.

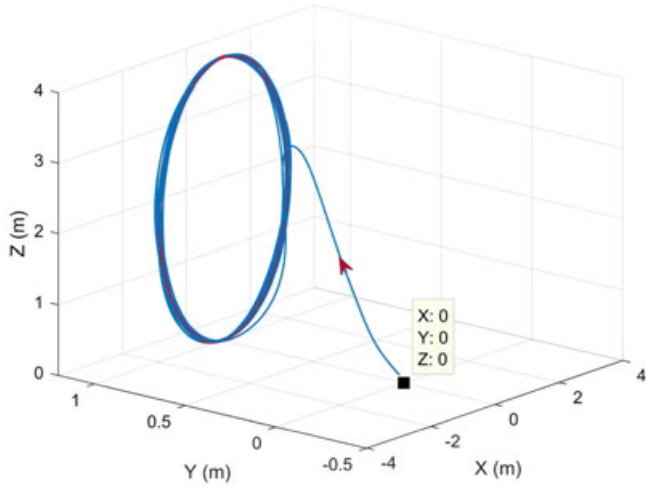

FIGURE 14 Path following in presence of wind [Colour figure can be viewed at wileyonlinelibrary.com]

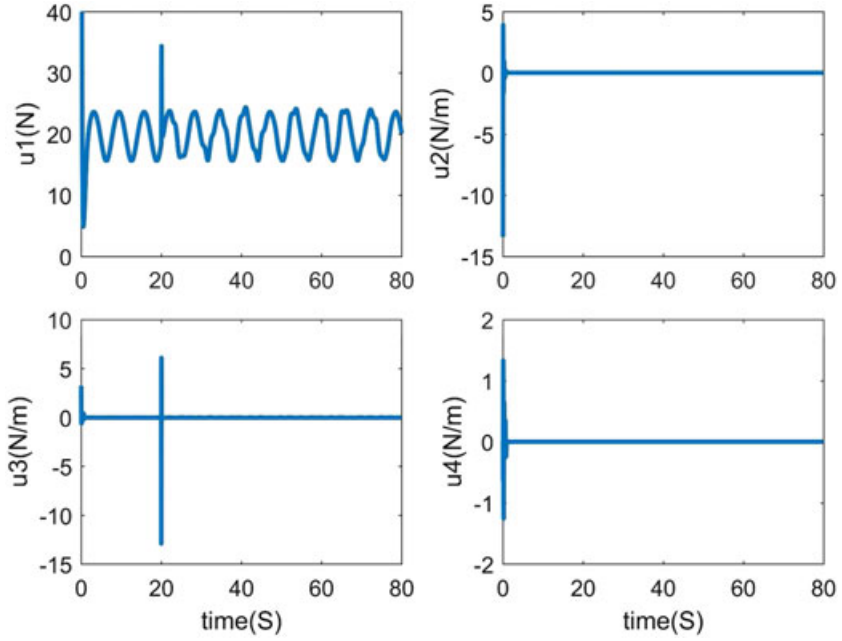

FIGURE 15 Control inputs in presence of wind [Colour figure can be viewed at wileyonlinelibrary.com]

5.2 | Simulation study subject to wind gust

The robustness of the designed control system against unmodeled dynamics is now evaluated (due to simplifications made in modeling). The initial condition and reference path are the same as the previous section. The control goal is to keep the robot on the path even in the presence of disturbance.

A disturbance, modeled as a wind with velocity $v_{\text{wind}} = \sin(0.8\pi t) + \cos(0.2\pi t) + \sin(0.4\pi t) + \cos(0.6\pi t)\,[1, 0, 0]'\ m/s$, has been applied to the robot after 20 seconds elapsed from the start time of the simulation. The results are demonstrated in Figures 14 and 15. As it is observed, the wind gust does not affect the tracking of position significantly. Figure 15 shows how the control inputs react to the disturbance. The controller has generated an adequate effort after 20 second (right at the point we apply the wind gust), to reject the multiharmonic disturbance.

6 | CONCLUDING REMARKS

The dynamic modeling and control of a modified quadrotor were studied in this article. The proposed configuration entails 4 control rotors and 2 constant speed coaxial propellers. This layout offers several advantages over a conventional quadrotor. The vehicle stability and capability to lift heavier payloads are improved while the dynamical behavior and steering principles are kept simple like a conventional quadrotor. Utilizing coaxial rotors enables the control motors spin at lower speeds as well. The physical parameters of the robot (used throughout the simulations) were measured experimentally. A hierarchical nonlinear control method based on the Lyapunov stability was used for position and attitude tracking control of the robot in 2 separate loops. The dynamical model of the quadrotor along with the controllers was simulated within MATLAB/SIMULINK. Results confirm that the proposed controller is able to move the aerial vehicle on a desired curved path even in the presence of wind disturbance. Also, the control inputs are smooth and bounded; therefore, they are quite feasible to be generated by means of existing actuators.

REFERENCES

1. Ollero AB, Merino LS. Control and perception techniques for aerial robotics. *Annu Rev Control*. 2004;28:167-178.
2. Cabecinhas D, Cunha R, Silvestre C. A nonlinear quadrotor trajectory tracking controller with disturbance rejection. *Control Eng Pract*. 2014;26:1-10.
3. Bouabdallah S, Noth A, Siegwart R. PID vs LQ control techniques applied to an indoor micro quadrotor. In Proceedings International Conference on Intelligent Robots and Systems. Sendai, Japan: IEEE; 2004:2451-2456.
4. Salih AL, Moghavvemi M, Mohamed HAF, Gaeid KS. Flight PID controller design for a UAV quadrotor. *Sci Res Essays*. 2010;5:8.
5. SA, Al-Hiddabi. Quadrotor control using feedback linearization with dynamic extension. In Proceeding of the 6th International Symposium on Mechatronics and its Applications, Sharjah, UAE, 2009.
6. Lee D, Kim H, Sastry S. Feedback linearization vs. adaptive sliding mode control for a quadrotor helicopter. *Int J Control Autom*. 2009;7:419-428.
7. Ramirez-Rodriguez H, Parra-Vega V, Sanchez-Orta A. Robust backstepping control based on integral sliding modes for tracking of quadrotors. *J Intell Robot Syst*. 2014;73:51-66.
8. Mian AA, Daobo W. Modeling and Backstepping-based nonlinear control strategy for a 6 DOF quadrotor helicopter. *Chin J Aeronaut*. 2008;21:261-268.
9. Bo Z, Xian B, Zhang Y, Zhang X. Nonlinear robust sliding mode control of a quadrotor unmanned aerial vehicle based on immersion and invariance method. *Int J Robust Nonlinear Control*. 2015;25:3714-3731.
10. Zheng E-H, Xiong J-J, Luo J-L. Second order sliding mode control for a quadrotor UAV. *ISA Trans*. 2014;53:1350-1356.
11. Liu H, Danjun Li JX, Zhong Y. Robust attitude controller design for miniature quadrotors. *Int J Robust Nonlinear Control*. 2016;26:681-696.
12. Zou Y. Nonlinear robust adaptive hierarchical sliding mode control approach for quadrotors. *Int J Robust Nonlinear Control*. 2016;27(6):925-941.
13. Gautam D, Ha C. Control of a quadrotor using a smart self-tuning fuzzy pid controller. *Int J Adv Robot Syst*. 2013;10:1-14.
14. Baek SJ, Jeon YP, Cho UR, Park JH, Lee DJ. Intelligent control system design of a unmanned quadrotor robot. *Appl Mech Mater*. 2014;548:917-921.
15. Salazar S, Romero H. Modeling and real-time stabilization of an aircraft having eight rotors. Instituto de Investigacioneselectrocas, 2009.
16. Yang C, Yang Z, Huang X. Modeling and robust trajectory tracking control for a novel six-rotor UAV. *Math Probl Eng*. 2013;2013:1-12.
17. Sámano A, Castro R, Lozano R, Salazar S. Modeling and stabilization of a multi-rotor helicopter. *J Intell Robot Syst*. 2013;69:1-9.
18. Driessens S, Pounds PEI. Towards a more efficient quadrotor configuration. Presented at the IEEE/RSJ International Conference on intelligent Robots and Systems (IROS); Tokyo, Japan; 2013.
19. Cao J, Anvar A. Design, modelling and simulation of maritime UAV-VTOL flight dynamics. *Appl Mech Mater*. 2012;152:6.

20. Prouty RW. *Helicopter Performance, Stability and Control*. London, United Kingdom: Krieger Publishing Company; 2001.

21. Lara D, Romero G, Sanchez A. Robustness margin for attitude control of a four rotor mini-rotorcraft: case of study. *Mechatronics*. 2010;20(1): 143-152.

22. Wang L, Jia H. The trajectory tracking problem of quadrotor UAV: global stability analysis and control design based on the Cascade theory. *Asian J Control*. 2014;16:15.

23. Choi Y-C, Ahn H-S. Nonlinear control of quadrotor for point tracking: actual implementation and experimental tests. *IEEE/ASME Trans Mechatronics*. 2014;20(3):1179-1192.

24. Jardin MR, Mueller ER. Optimized measurements of UAV mass moment of inertia with a bifilar pendulum. Hilton Head, USA: Presented at the AIAA Guidance, Navigation Control USA; August 20-23, 2007.

25. Bertrand S, Guénard N, Hamel T, Piet-Lahanier H, Eck L. A hierarchical controller for miniature VTOL UAVs: Design and stability analysis using singular perturbation theory. *Control Eng Pract*. 2011;19:1099-1108.

How to cite this article: Tofigh MA, Mahjoob MJ, Ayati M. Dynamic modeling and nonlinear tracking control of a novel modified quadrotor. *Int J Robust Nonlinear Control*. 2017;1–15. https://doi.org/10.1002/rnc.3885